© 2018. Published by The Company of Biologists Ltd | Development (2018) 145, dev163477. doi:10.1242/dev.163477

RESEARCH ARTICLE

Bsx controls pineal complex development

Theresa Schredelseker[1,2] and Wolfgang Driever[1,2,*]

ABSTRACT

Neuroendocrine cells in the pineal gland release melatonin during the night and, in teleosts, are directly photoreceptive. During development of the pineal complex, a small number of cells migrate leftward away from the pineal anlage to form the parapineal cell cluster, a process that is crucial for asymmetrical development of the bilateral habenular nuclei. Here, we show that, throughout zebrafish embryonic development, the *brain-specific homeobox* (*bsx*) gene is expressed in all cell types of the pineal complex. We identified Bmp and Noto/Flh as major regulators of *bsx* expression in the pineal complex. Upon loss of Bsx through the generation of a targeted mutation, embryos fail to form a parapineal organ and develop right-isomerized habenulae. Crucial enzymes in the melatonin biosynthesis pathway are not expressed, suggesting the absence of melatonin from the pineal gland in *bsx* mutants. Several genes involved in rod-like or cone-like phototransduction are also abnormally expressed, indicating that Bsx has a pivotal role in the differentiation of multiple cell types in the zebrafish pineal complex.

KEY WORDS: Bsx, *Brain-specific homeobox* transcription factor, Pineal gland, Parapineal organ, Habenula, Epithalamus, Photoreceptors, Brain asymmetry, Melatonin

INTRODUCTION

Development of the epithalamus, which comprises the pineal complex (PC) in the dorsal midline of the diencephalon and the flanking paired habenulae, has long fascinated developmental biologists because of both the formation of left-right asymmetrical anatomical structures and light-regulated melatonin synthesis in the pineal system (Concha and Wilson, 2001; Duboc et al., 2015; Roberson and Halpern, 2018; Sapède and Cau, 2013). In mammals, information about light conditions reaches the pineal gland (PG) via the retina and suprachiasmatic nucleus, whereas the PG of poikilothermic vertebrates is directly photoreceptive (Dodt, 1973).

The PC comprises the dorsomedial PG and the adjacent parapineal organ (PP). During zebrafish embryonic development, cells from the anterior part of the pineal anlage migrate away from the midline to form the PP, which, in >95% of wild-type embryos is located on the left side (Concha et al., 2000). Laser ablation studies revealed that unilateral PP formation is necessary for asymmetric development of the habenulae (Gamse et al., 2003). Habenula asymmetry is not only reflected in differential gene expression on the left and right sides, but is also apparent in different efferent projections of the two lobes (reviewed in Duboc et al., 2015). Functional implications of habenula laterality were recently demonstrated through right-isomerized zebrafish showing aberrant behavior (Facchin et al., 2015).

The first transcription factor to be identified as being crucial for proper PG development was Floating head (Flh/Noto). The expression domain of *flh* in the PG is specified by Wnt along the anterior-posterior axis (Masai et al., 1997), and by Bmp along the dorsoventral axis (Barth et al., 1999). Tbx2b, which was previously implicated in retinal photoreceptor (PhR) cell differentiation (Gross and Dowling, 2005), has been proposed to specify premigratory PP cells in the anterior part of the pineal anlage (Snelson et al., 2008a,b). Subsequently, in an Fgf8a-dependent mechanism, those cells migrate leftward away from the midline to form the PP cell cluster (Regan et al., 2009; Clanton et al., 2013). Pitx2c, a target of Nodal signaling, restricts the number of PP cells (Garric et al., 2014). Most recently, Nr2e3, another transcription factor with a long-established role in retinal PhR cell specification (Akhmedov et al., 2000), was described as a positive regulator of PG cells and a negative regulator of PP cell fate (Khuansuwan et al., 2016).

Although a small structure, the exact identity and number of different cell types within the teleost PC in adult and larval stages is still disputed. Based on morphological features, pineal PhR cells in the adult teleost are difficult to classify into rod-like or cone-like types because of their rudimentary outer segments (Meissl and Yáñez, 1994). In the larval PG, PhR cell morphology is even less well characterized. However, building on distinct gene expression profiles of rod and cone cells in the retina, discrimination between PhR cell types in the early larval PG is frequently based on the expression of genes involved in retinal rod- or cone-specific phototransduction (Lagman et al., 2015). Apart from PhR cells, the teleost PG harbors neurons that form long and extensively arborizing projections to both diencephalic and mesencephalic nuclei (Yáñez et al., 2009). Most recently, cells expressing *agouti-related peptide 2* (*agrp2*) were suggested to be a novel cell type in the larval zebrafish PG (Shainer et al., 2017). Despite their crucial and well-described role in the establishment of left-right asymmetry, functional characterization of PP cells is sparse. However, recent transcriptome analyses suggest that PP cells represent a specialized form of PhR cells (Khuansuwan and Gamse, 2014).

Here, we studied the Brain-specific homeobox (BSX) transcription factor, which is highly conserved among vertebrates (Fig. S1A). Mammalian *Bsx* transcripts have been demonstrated to be expressed in the developing PG, ventral hypothalamus and telencephalic septum (Cremona et al., 2004). BSX in the hypothalamus is required for normal expression levels of two genes encoding potent orexigenic neuropeptides: *agouti-related neuropeptide* (*Agrp*) and *neuropeptide Y* (*Npy*) (Sakkou et al., 2007). Data on the role of BSX in PG development and function are sparse: PG hypoplasia in *Bsx* mutant mice has been described but not characterized in detail (McArthur and Ohtoshi, 2007) and a role for Bsx in pineal PhR cell differentiation has been suggested (D'Autilia et al., 2010).

[1]Developmental Biology, Institute Biology I, Faculty of Biology, Albert-Ludwigs-University Freiburg, Hauptstrasse 1, 79104 Freiburg, Germany. [2]BIOSS - Centre for Biological Signalling Studies, Schänzlestrasse 11, 79104 Freiburg, Germany.

*Author for correspondence (driever@biologie.uni-freiburg.de)

T.S., 0000-0001-9965-7712; W.D., 0000-0002-9551-9141

Received 16 January 2018; Accepted 8 June 2018

Development (2018) 145, dev163477. doi:10.1242/dev.163477

We detected zebrafish *bsx* expression in anatomical domains corresponding to those described in mice. We explored Bsx functions in epithalamus development and integrate Bsx into the current regulatory network underlying PC development. Bsx is required for PP cell specification and, thus, is crucial for asymmetric development of the habenulae. In addition, Bsx is required for proper differentiation of PhR cells and neuroendocrine melatonin-releasing pinealocytes.

RESULTS

bsx is expressed in the pineal complex and hypothalamus throughout embryonic development

Performing whole-mount *in situ* hybridization (WISH), we found *bsx* in zebrafish embryos to be first expressed during the mid-somitogenesis stages [10 somites, 14 h post fertilization (hpf); Fig. 1A], correlating with late neurulation. The earliest *bsx* expression domain was detected in the dorsal-most part of the diencephalon in the pineal anlage area (Fig. 1A, arrow and A′), and had become more compact by the 20-somite stage (19 hpf; Fig. 1B,B′) and 24 hpf (Fig. 1C,C′). At ∼30 hpf, *bsx* expression had become asymmetric (Fig. 1D,D′), indicating that *bsx* is expressed in both medially located PG cells and leftward migrating PP cells. PC *bsx* expression persisted during both embryonic and larval development (Fig. 1E-I′).

Another *bsx* expression domain in the presumptive hypothalamus became apparent during mid-somitogenesis, initially comprising a few scattered cells (10-somite stage; Fig. 1A, arrowhead). *bsx*-expressing cell clusters formed in the ventral and caudal hypothalamus as well as in the rostral hypothalamus/prethalamus region (Fig. 1D-I). At ∼24 hpf, a few cells started to express *bsx* in the ventral telencephalon, which, during the second day of development, formed a domain that was likely to be located in the septal region, based on comparison with data from mice (Cremona et al., 2004). *bsx* expression in the forebrain persisted throughout all the larval stages assessed (until 5 days post fertilization; dpf).

Although *Bsx* expression in both the PG and hypothalamus of mice has been described previously (Cremona et al., 2004), our work revealed asymmetric *bsx* expression in the zebrafish PC. Only one study had previously addressed the molecular function of Bsx in the PG, revealing strong circadian rhythmicity in expression of *bsx* in *Xenopus laevis* larvae, with high expression levels during the night and almost no expression during the day (D'Autilia et al., 2010). However, in zebrafish, we found little or no circadian variation in *bsx* expression and no significant differences in expression levels when comparing light-entrained embryos with embryos raised in darkness (Fig. S2), suggesting different Bsx functions in amphibians compared with teleosts.

bsx is expressed in all cell types of the pineal complex

To reveal which cell types of the PC express *bsx*, we performed double-fluorescent WISH. We found that *bsx* is co-expressed with *exorhodopsin* (*exorh*), a marker of rod-like PhR cells (Fig. 2A-A″), and the *gnat2* gene, encoding cone-specific G protein-transducing alpha subunit (Fig. 2B-B″), indicating that *bsx* is present in both rod- and cone-like PhR cells. A well-studied function of the PG is the release of melatonin during the night. Thus, we assessed the co-expression of *bsx* and *tryptophan hydroxylase 1a* (*tph1a*), encoding a key enzyme in the synthesis of the melatonin precursor serotonin. Co-expression of both genes (Fig. 2C-C″) indicated that melatonin-releasing cells express *bsx*. We also found *bsx* transcripts in cells expressing *agrp2* (Fig. 2D-D″), which were recently proposed as a novel pineal cell type (Shainer et al., 2017). Colocalization of *bsx* and *gfi1ab* transcripts demonstrated *bsx* expression in not only PG cells, but also PP neurons (Fig. 2E-E″). To test whether *bsx* is also expressed in developing pineal PNs, we used *elavl3* as a marker to label these neurons (Cau et al., 2008). We found *bsx* to be colocalized with *elavl3* (Fig. 2F-F″), indicating that at least a subset of PNs also express *bsx*. From these experiments, we conclude that cells of each major cell type in the PC express *bsx*.

Although *elavl3*-expressing PNs have been described to be located mainly in two lateral fields within the PG (Cau et al., 2008), we noted that additional cell types might preferentially cluster in subregions of the PG (Fig. 2). When analyzing *z*-projections of confocal image stacks (Fig. S3), we found photoreceptive cells

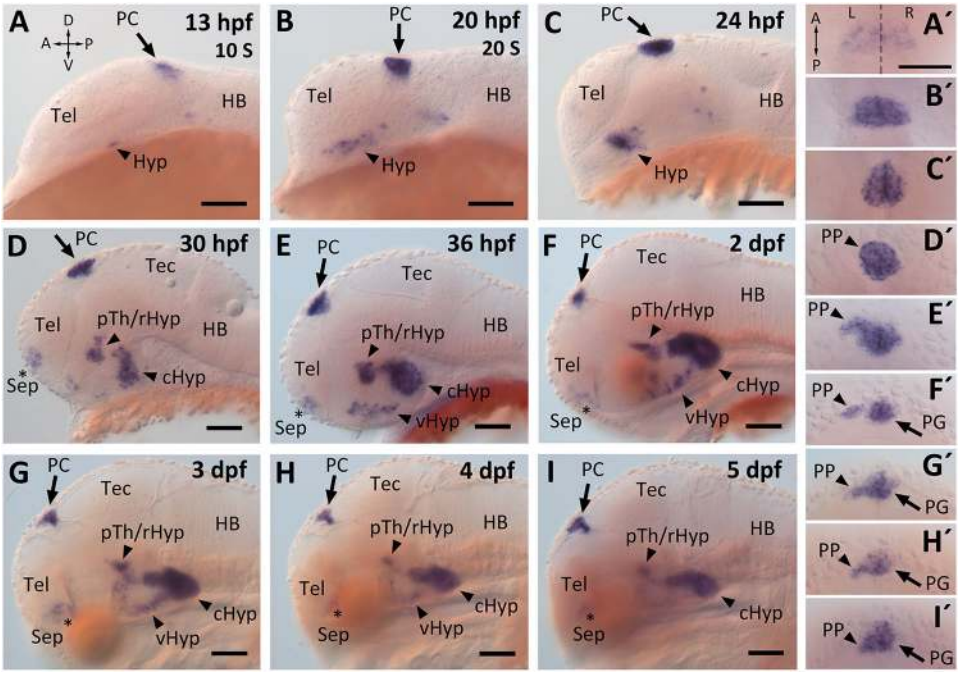

Fig. 1. *bsx* expression during zebrafish embryonic development. (A-I′) *bsx* expression visualized by WISH. (A-I) Lateral views of head region of zebrafish embryos, and (A′-I′) dorsal views of the PC of the same embryos. Developmental stages (S, somite stage) and orientations (A, anterior; D, dorsal; L, left; P, posterior; R, right; V, ventral; dashed line indicates the midline) are indicated. HB, hindbrain; Hyp, hypothalamus (c, caudal; r, rostral; v, ventral); pTh, prethalamus; Sep, septal region; Tec, midbrain tectum; Tel, telencephalon. Scale bar: 100 µm.

Development (2018) 145, dev163477. doi:10.1242/dev.163477

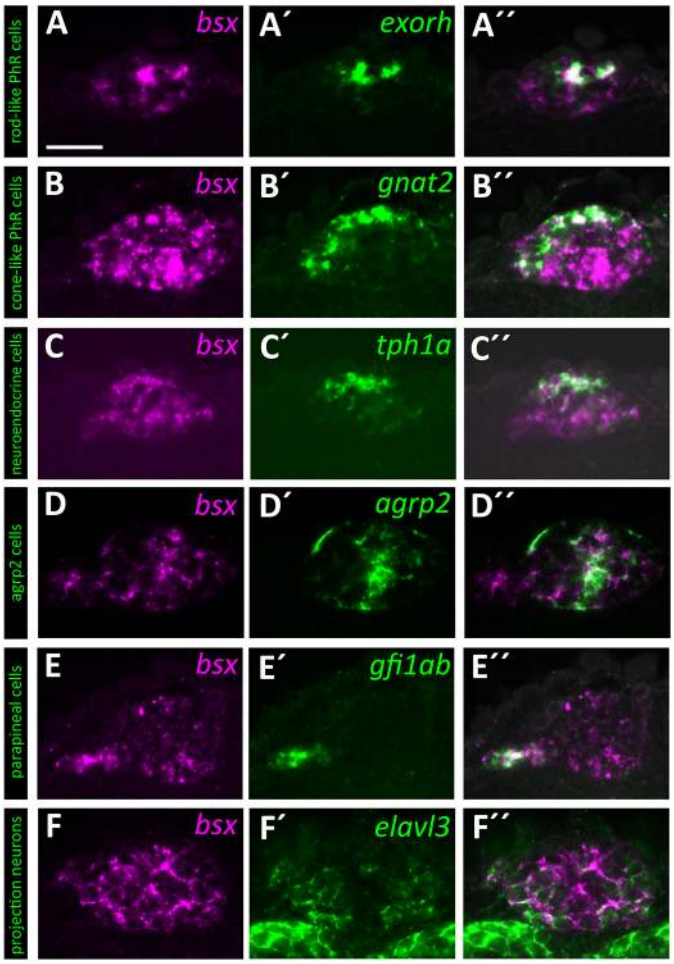

Fig. 2. *bsx* is expressed in all cell types of the PC except projection neurons. (A-F″) Double-fluorescent WISH of 3 dpf wild-type zebrafish embryos detects expression of *bsx* (magenta, A-F), PC type-specific marker genes (as indicated in green, A′-F′), and merged channels (A″-F″). All panels show single confocal planes (image depth *z*=1 µm; anterior is to the top). $n \geq 2$ for all. Maximum intensity projections of stacks are shown in Fig. S3. Scale bar: 20 µm.

clustered in the anterior part of the PG, whereas *agrp2*-expressing cells were distributed more evenly, with a slightly stronger accumulation along the midline in the posterior part of the PG. We integrated these observations into a model of PC cellular organization (Fig. 8B).

Bmp but not Wnt signaling acts upstream of *bsx* in the pineal complex

The pineal anlage is specified along the anterior-posterior axis by Wnt (Masai et al., 1997), and along the dorsoventral axis by Bmp (Barth et al., 1999). Using *Tg(hsp70l:Wnt8a-GFP)*, we overexpressed a Wnt8a-GFP fusion protein by heat-shock treatment from 12 to 13 hpf to induce canonical Wnt signaling and to test whether the pineal *bsx* expression domain expands throughout the dorsal forebrain. However, when analyzed at 16 hpf, we found *bsx* expression in the pineal anlage to be unaffected by high levels of Wnt8a (Fig. 3A,B). As a control, and in accordance with the literature (Masai et al., 1997), we confirmed that heat-shock Wnt8a overexpression strongly expanded the *flh* expression domain anteriorly (Fig. 3C,D). Inhibition of Wnt signaling by the chemical inhibitor IWR-1 exerted no effect on the pineal *bsx* expression domain (Fig. 3E,F), whereas a substantial downregulation of *flh* expression was observed (Fig. 3G,H). We conclude that *bsx* expression in the pineal anlage is not regulated by Wnt signaling.

We analyzed the effect of Bmp overexpression on *bsx* expression by applying heat-shock from 12 to 13 hpf to *Tg(hsp70l:bmp2b)* embryos. We found *bsx* expression in the pineal region at 24 hpf to be expanded not only ventrally, but also along the anterior-posterior axis (Fig. 3I-J′). Conversely, inhibition of Bmp signaling through 12 to 13 hpf by heat-shock-driven overexpression of a dominant-negative Bmp receptor from *Tg(hsp70l:dnXla.Bmpr1a-GFP)* resulted in a reduction of *bsx* expression in the pineal anlage at 24 hpf (Fig. 3K-L′).

Given that *bsx* expression starts around the time when the pineal anlage fuses at the midline (Fig. 1A,A′), we assessed whether neural tube closure is necessary for *bsx* expression. We found that, in *lefty1*-injected embryos, in which the neural tube fails to close, *bsx* was expressed bilaterally in the epithalamus (Fig. S4A,B). This indicates that neural tube closure is not necessary for *bsx* expression in the pineal anlage. Later in development, left-sided Nodal signals act as positional cues to direct the PP to the left side (Concha et al., 2000; Liang et al., 2000). In accordance with this model, we found sidedness of PP *bsx* expression to be randomized in *ntl*/*ta* mutant embryos, which lack midline structures thought to represent a diffusion barrier for Nodal (Concha et al., 2000; Fig. S4C,D).

Bsx is required for parapineal formation and habenula asymmetry

To analyze the role of Bsx in the PC, we used Transcription Activator-like Effector Nucleases (TALENs) to establish a genetic *bsx* loss-of-function mutation. Using a previously described TALEN pair (Sander et al., 2011), we targeted the homeobox of *bsx*. Sequencing the targeted genomic region in F2 animals revealed an indel (25 bp deletion and 5 bp random insertion) leading to a frame shift after 114 amino acids, and introducing a premature stop codon after 14 additional amino acids. This bsx^{m1376} allele was predicted to express a truncated Bsx protein lacking most of its DNA-binding homeodomain (Fig. S1D). We compared the biological activities of *bsx* wild-type and bsx^{m1376} synthetic mRNAs by microinjection at the one-cell stage. We found that overexpression of wild-type *bsx* mRNA strongly impeded early development, whereas bsx^{m1376} mRNA did not interfere with normal development (Fig. S5). Hence, bsx^{m1376} is considered a null allele.

To investigate potential pineal morphogenesis and differentiation defects in *bsx* mutant larvae, we made use of *otx5* as a marker for PC cells adopting a PhR cell fate (Gamse et al., 2002). *otx5* expression was reduced in the PG of *bsx* mutants and a domain corresponding to the PP was not detected (Fig. 4A,A′ arrowheads). In agreement, we found PP cell-specific *gfi1ab* expression to be completely absent in *bsx* mutant larvae (Fig. 4B,B′ arrowheads). In *fgf8a* and *tbx2b* mutants, the PP cell cluster was not established on the left side of the brain, and cells expressing PP-specific genes were still present but failed to be displaced from the midline, indicating a migration defect (Regan et al., 2009; Snelson et al., 2008b). By contrast, failure to detect any PP-specific gene expression suggested an early specification defect in *bsx* mutants. To test this possibility, we followed GFP^+ cells in *Tg(foxd3:GFP)*, which marked early PP cells forming at the midline in the anterior part of the pineal anlage before 34 hpf, and migrating to the left over the following 12 h. However, in *bsx* mutant embryos, PP cells expressing GFP did not form at 34 hpf or later (Fig. 4H). The absence of PP cells at this early specification stage was confirmed by the lack of *sox1a* expression in the PC of *bsx* mutants at 30 hpf (Fig. S6), when *sox1a* is a marker of premigratory PP cells (Clanton, 2013; Khuansuwan et al., 2016). In addition, *LIM homeobox 2b* (*lhx2b*) expression, which is detected at the onset of PP cell migration (Clanton, 2013), is reduced in *bsx* mutants (Fig. 4C,C′ arrowheads).

Development (2018) 145, dev163477. doi:10.1242/dev.163477

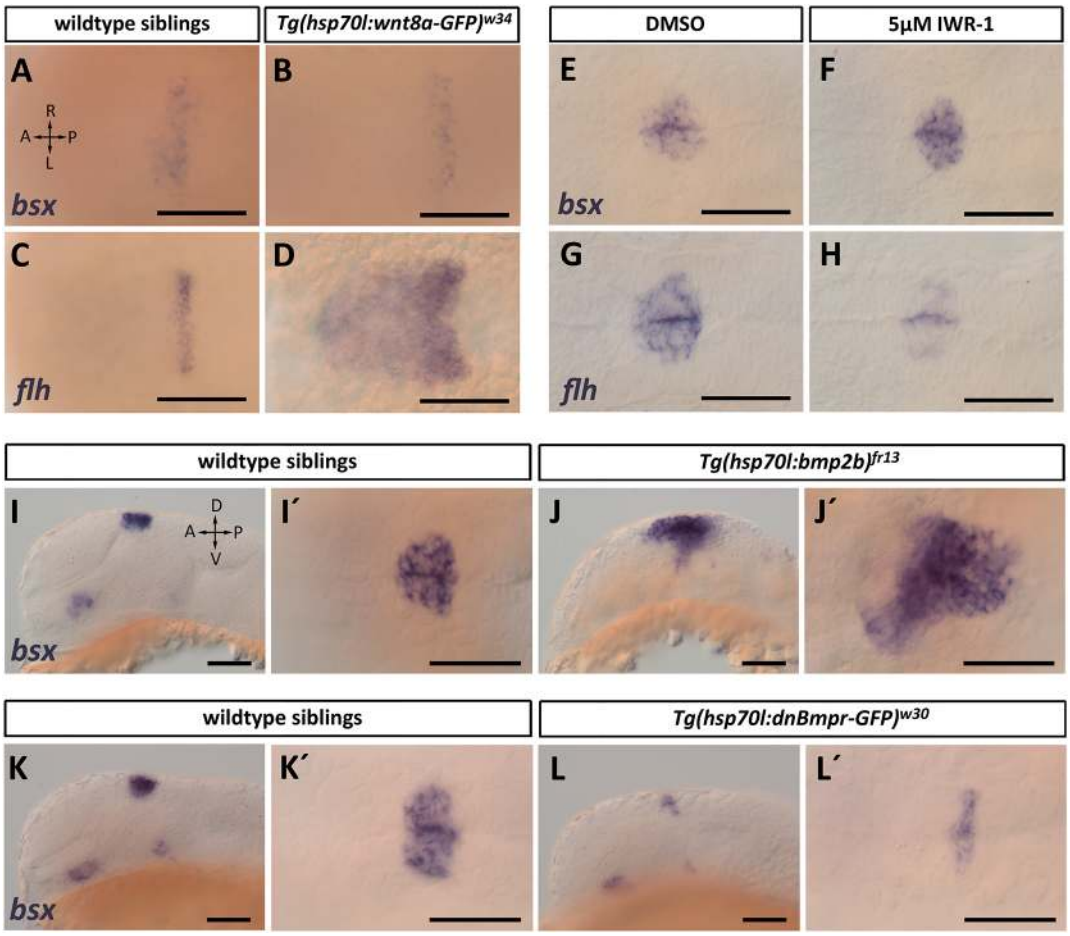

Fig. 3. Bmp but not Wnt signaling regulates *bsx* expression in the PC. (A-D,I-L′) Transgenic embryos (as indicated in boxes) and wild-type control siblings were heat-shocked for 1 h from 12 to 13 hpf and fixed either at 16 hpf (A-D) or 24 hpf (I-L′). (E-H) Embryos were treated with the Wnt inhibitor IWR-1 from 2 hpf onwards and fixed at 24 hpf. *bsx* or *flh* expression were detected by WISH as indicated. (A-H,I′,J′,K′,L′) Dorsal views, orientations as indicated in (A); (I,J,K,L) lateral views, orientations as indicated in (J). Numbers for representative phenotype shown and embryos analyzed: (A) 19/19, (B) 20/20, (C) 14/14, (D) 17/17, (E) 18/18, (F) 14/14, (G) 19/19, (H) 13/15, (I,I′) 26/26, (J,J′) 27/27, (K,K′) 16/16 and (L,L′) 15/16. Scale bars: 100 µm.

Formation of the PP in the left epithalamus was previously demonstrated to be necessary for the establishment of habenula asymmetry in wild-type larvae: laser ablation of the PP cells before or during migration results in right-isomerized habenulae (Gamse et al., 2003). In line with these results, *bsx* mutant larvae developed double-right-sided habenulae, as detected by the symmetric expression of *potassium channel tetramerization domain-containing 12.1* (*kctd12.1*) and *kctd12.2* genes (Fig. 4D-E′). Habenula right isomerization in *bsx* mutant embryos was confirmed by the absence of *adenylate cyclase-activating polypeptide 1a* (*adcyap1a*) expression, which, in wild-type embryos, is expressed in the left habenula only (Fig. 4F,F′), and by bilateral expression of *slc18a3b* (*vesicular acetylcholine transporter*; Fig. 4G,G′), a cholinergic gene that, in wild-type embryos, is expressed at higher levels in the right habenula (Hong et al., 2013).

Taken together, our data suggest an early defect in PP development, subsequently leading to habenula right isomerism. We note that, in addition to PP absence, *otx5* and *lhx2* expression is also reduced in the PG (Fig. 4A,A′,C,C′), suggesting not only PP, but also PG defects in *bsx* mutants.

Bsx position in the pineal complex transcriptional network

Upon loss of *flh* expression, pineal neurogenesis is impaired (Masai et al., 1997). We found *bsx* expression in *flh* mutants to be substantially downregulated (Fig. 5A,B). This indicates that *bsx* expression in the PC is, to some extent, dependent on Flh. Conversely, *flh* expression was normal in *bsx* mutants (Fig. 5G,H), suggesting that Bsx does not regulate *flh*. Another transcription factor acting downstream of Flh in PC differentiation, *otx5*, was downregulated in the PG of *bsx* mutants (Fig. 4A,A′). Using a previously described morpholino (MO) for *otx5* knockdown (Gamse et al., 2002), we found *bsx* to be expressed normally upon knock down of Otx5 (Fig. S7A-D). These results indicate that *otx5* is regulated by Bsx, but not vice versa. As previously shown, *otx5* transcript levels are reduced and displaced from the midline in *flh* mutants (Gamse et al., 2002). We analyzed the interplay between *flh* and *bsx* in double mutants. We found that, whereas loss of either Bsx or Flh was sufficient to substantially reduce the expression of *otx5* (Fig. 5C-E), loss of both Bsx and Flh was required for complete absence of *otx5* transcripts from the PC (Fig. 5F). This indicates that Bsx and Flh provide partially redundant parallel input into *otx5* regulation in PhR cell specification.

Next, we assessed a potential connection between Bsx and other transcriptional regulators implicated in PP specification. Expression of *nr2e3* in *bsx* mutants appeared to be unaffected (Fig. 5K,L). Likewise, *bsx* expression was not substantially altered upon knock down of *nr2e3* (Fig. S7H), indicating that Bsx and Nr2e3 do not regulate the expression of the other, but rather act in parallel. Also,

Development (2018) 145, dev163477. doi:10.1242/dev.163477

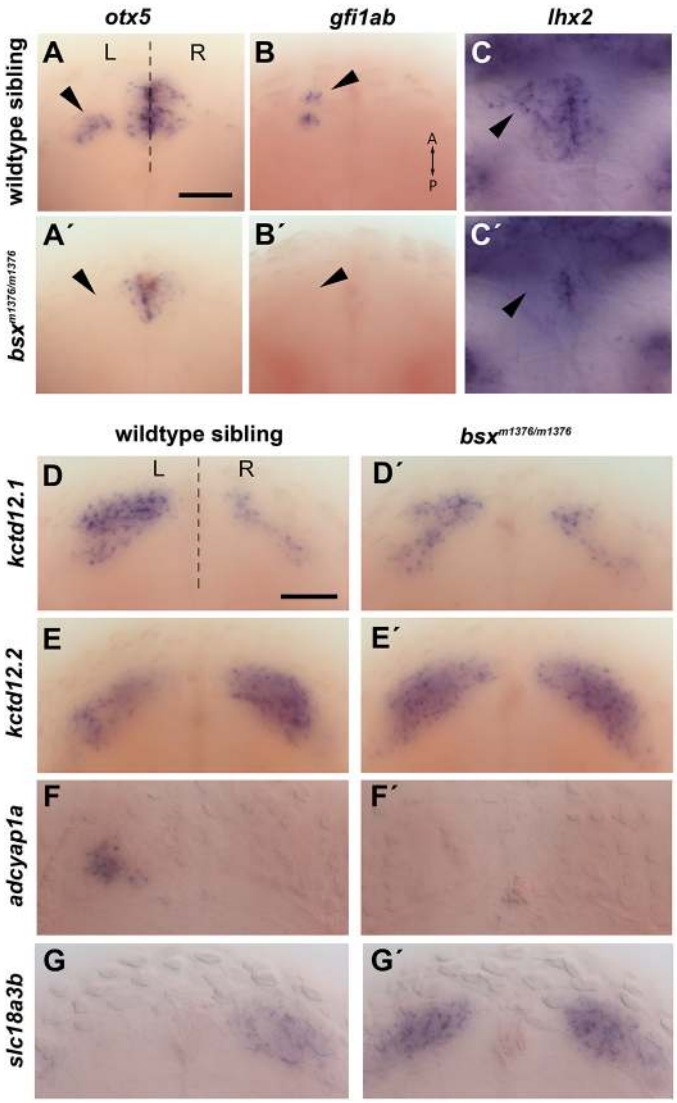

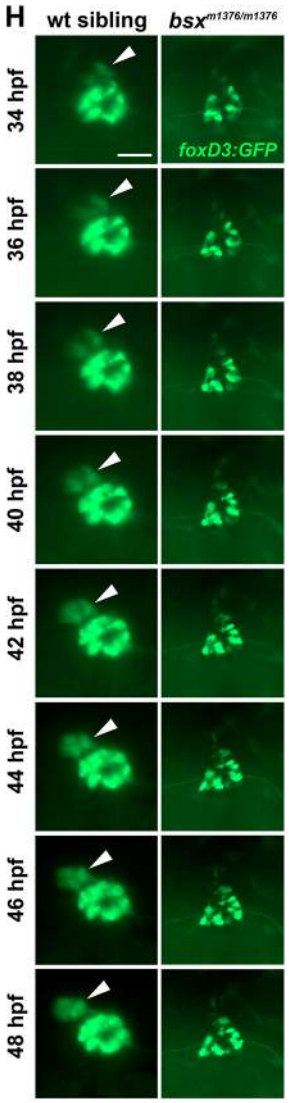

Fig. 4. Absence of parapineal cell cluster and habenula right-isomerism in embryos homozygous for a targeted *bsx* mutant allele. (A-G) Expression of PC or habenula markers analyzed by WISH in wild-type and *bsx* mutant embryos at 3 dpf (A-B′,D-E′,G,G′), 34 hpf (C,C′) or 5 dpf (F,F′). Arrowheads indicate the location of PP cells. All embryos were genotyped [$n \geq 4$ each for wild type (wt) and mutants]. Dorsal views, with the anterior at the top. (H) Time series of pineal anlage in *Tg(foxd3:GFP)* at stages (indicated at left) when the PP develops. In wt but not *bsx* mutant embryos, GFP^+ cells migrate out of the anterior pineal anlage to form a PP cell cluster (arrowhead). Widefield epifluorescence images (20× lens, NA 1.0) of PC, dorsal views, with the anterior at the top. L, left; R, right. Scale bars: 100 µm (A-G) and 50 µm (H).

expression of *tbx2b* was normal in *bsx* mutants (Fig. 5M,N). However, when knocking down *tbx2b* expression by MO injection, we found no or only very few bsx^+ PP cells displaced from the medial PG (Fig. S7F). This result is consistent with a previously published report showing both a decreased number and migration failure of PP cells upon knock down of *tbx2b* (Snelson et al., 2008b).

Next, we analyzed the interplay between *bsx* and *pitx2c*, a Nodal target expressed in the left diencephalon, which has been shown to regulate PP cell number (Garric et al., 2014). We found left-side-specific expression of *pitx2c* to be normal in *bsx* mutants (Fig. 5O,P) and *bsx* expression not to be altered in *pitx2c* morphants (Fig. S7G). Thus, we hypothesize that Bsx and Pitx2c determine PP cell fate largely independent of each other.

Fgf8a signaling is crucial for migration of PP cells to the left (Regan et al., 2009; Clanton et al., 2013). In line with this, we found no *bsx* expression displaced from the midline in hypomorphic $fgf8a^{ti282a}$ mutants (Fig. S7J,K). Given that we detected no difference in *fgf8a* expression between *bsx* mutants and wild type (Fig. 5Q,R), we conclude that *fgf8a* expression is independent of Bsx. Thus, both Bsx and Fgf8a appear to be necessary for the establishment of a left-positioned PP, but one factor does not substantially influence the expression of the other. Furthermore, we found that, in *bsx* mutant embryos, the absence of PP cells was also apparent through loss of *bsx* expression left of the PG but that *bsx* expression was not affected in the PG cells themselves (Fig. 5I,J). This indicates that Bsx activity is not required to maintain *bsx* expression. In conclusion, our data establish Bsx as an important factor in the pineal transcriptional specification network that is necessary for PP cell fate, and is expressed mostly independent of previously described PC transcription factors, except Flh.

Bsx is necessary for the correct differentiation of all cell types in the pineal gland

Both *otx5* and *lhx2* have been implicated in PhR cell differentiation (Gamse et al., 2002; Gordon et al., 2013; Roy et al., 2013). Given that the expression of both genes is substantially downregulated in *bsx* mutants, we analyzed formation of the different pineal cell types using *Tg(foxD3:GFP)* (Gilmour et al., 2002), which has been suggested to label PP cells, PNs and cone-like PhR cells in the PG (Clanton et al., 2013). We also assessed Arr3a immunoreactivity, which has been described as a cone-specific marker (Larison and Bremiller, 1990). We found no Arr3a immunoreactivity in *bsx* mutants, and the expression of GFP from *Tg(foxD3:GFP)* to be significantly reduced in *bsx* mutants (Fig. 6A,B).

To further characterize the extent to which the different pineal cell types are affected by Bsx loss, we performed double-

Development (2018) 145, dev163477. doi:10.1242/dev.163477

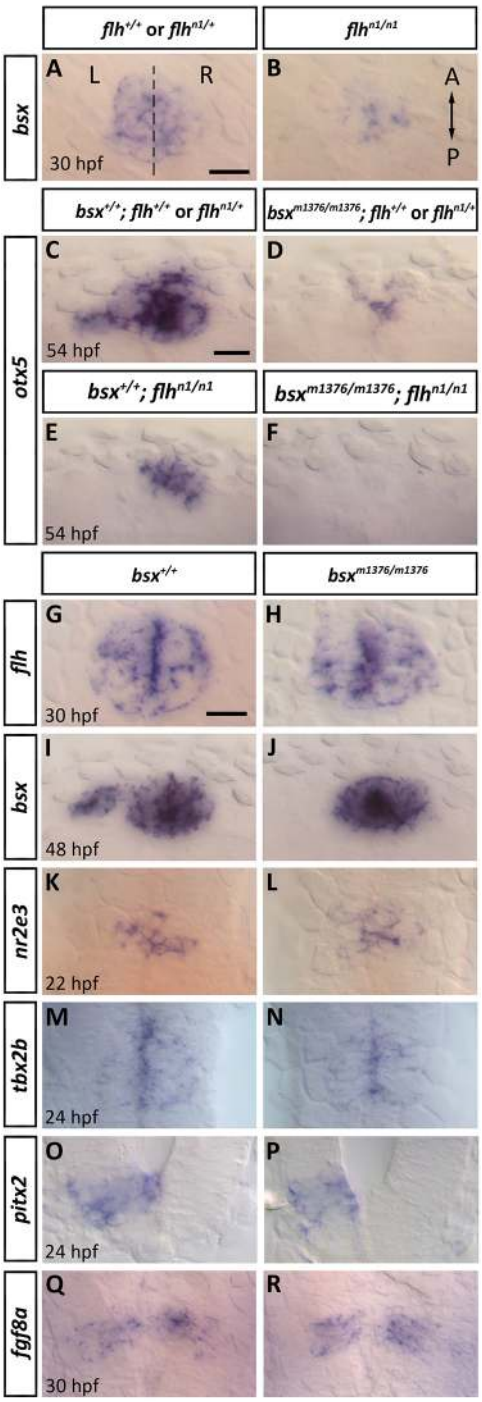

Fig. 5. Epistatic positioning of *bsx* in the PC transcriptional network. (A-R) Expression of mRNAs encoding PC transcription factors or signals analyzed by WISH at indicated stages. Genotypes of embryos were wild type, single, or double mutant for *bsx* and *flh*, as indicated at top. The genes for which expression was analyzed are given on the left. Anterior is to the top of the images. Analyzed embryos $n \geq 3$ for wild type, $n \geq 4$ for *bsx* or *flh* single mutants and $n \geq 2$ for *bsx*/*flh* double mutants. Scale bars: 20 µm.

immunolabeling of GFP and Elavl3/HuC in *Tg(foxD3:GFP)* embryos and counted cells (Fig. 6C-D‴, Movie 1). We found that the number of GFP$^+$ cells was drastically reduced in *bsx* mutants (15.1±2.9 compared with wild type 82.7±7.0, mean±s.d.; Fig. 6E,F and Table S3). The number of HuC$^+$ cells was also significantly reduced in *bsx* mutants (27.9±4.4 compared with wild type 46.9±3.3). In wild-type embryos, approximately half of the GFP$^+$ cells did not express HuC (37.6±6.2), whereas, in *bsx* mutants, there are very few such cells (0.7±1.5). That most of the remaining GFP$^+$ cells in *bsx* mutants were HuC$^+$ supports the hypothesis that most of the GFP$^+$ cells in *bsx* mutants are PNs. In addition to reduced cell numbers in *bsx* mutants, we also observed that remaining PNs in *bsx* mutants did not form lateral clusters but tended to be located only in the caudal-most part of the PG (Fig. 6D′, Movie 1). We observed axonal projections originating from the GFP$^+$ cells in *bsx* mutants, indicating that these cells correspond to PNs (Fig. 6G-H). However, the PN neurites frequently formed supernumerary and morphologically abnormal branches compared with wild type (Fig. 6G-I).

To determine the formation of neuroendocrine pinealocytes, we analyzed PG expression of enzymes involved in melatonin production. We found that expression of *arylalkylamine* N-*acetyltransferase 2* (*aanat2*) (Fig. 6J,K) and of *tph1a* and *tph2* (Fig. 6L-O; Fig. S8) was completely absent in *bsx* mutants. This suggests that the PG of *bsx* mutants is unable to produce both melatonin and its precursor, serotonin. Furthermore, expression of *agrp2* was strongly reduced in *bsx* mutants (Fig. 6P,Q).

Loss or reduction of PG cell types can be caused by apoptosis; therefore, we performed terminal deoxynucleotidyl transferase dUTP nick end labeling (TUNEL) assays at 30 hpf or 72 hpf, but found no evidence of increased apoptosis in the PC of *bsx* mutants (Fig. S9). Thus, loss of specific cell types could be caused by mis-specification or abnormal differentiation rather than by cell death.

Bsx specifies photoreceptor subtypes in the pineal gland and inhibits UV-cone development

Next, we investigated Bsx activities in cone differentiation. For most of the marker genes analyzed, we did not detect complete elimination of expression, but variation in WISH stain intensity or area (Fig. 7A). To identify subtle, but significant changes, we quantified the staining intensity of our WISH data through background-adjusted measurements of integrated density in the PG (Fig. 7B, Materials and Methods, Fig. S10) of genotyped embryos. We analyzed the expression of the cone-specific G-protein transducin alpha and gamma subunits *gnat2* and *gngt2a*. Interestingly, we found *gnat2* expression to be normal in *bsx* mutants, whereas that of *gngt2a* was downregulated. We further analyzed the expression of the cone-specific *recoverins* (*rcv*) *rcv1b*, *rcv2a* and *rcv2b* and detected a significant downregulation of each of them in *bsx* mutants. Given that Arr3a, for which we demonstrated the absence of both the protein (Fig. 6A) and transcripts (Fig. 7A) in the PG of *bsx* mutants, has been shown to be red/green double cone specific (Renninger et al., 2011), we investigated whether cones with different spectral sensitivity are differentially affected upon loss of Bsx. Thus, we analyzed the expression of the UV- and blue-cone-specific *arrestin 3b* (*arr3b*) in *bsx* mutants, and found expression levels to be similar to wild type. Even more strikingly, we found the UV-sensitive *opsin 1 (cone pigments), short-wave-sensitive 1* (*opn1sw1*) to be expressed in *bsx* mutants, whereas it was not expressed in wild-type PGs in the larval stages. However, when we assessed the expression of *rcv1a*, which is specific to UV cones and rods (Zang et al., 2015), we observed a significant downregulation in *bsx* mutants. This result suggests that rod-like PhR cells are also affected in *bsx* mutants. However, similar to the cone-specific transducin subunits, the rod-specific alpha subunit *gnat1* was unchanged in *bsx* mutants, whereas the gamma subunit *gngt1* was downregulated. Remarkably, we found the rod-specific opsins *rhodopsin* (*rho*) and *exorh* to be significantly upregulated in *bsx* mutants (Fig. 7A,B).

Development (2018) 145, dev163477. doi:10.1242/dev.163477

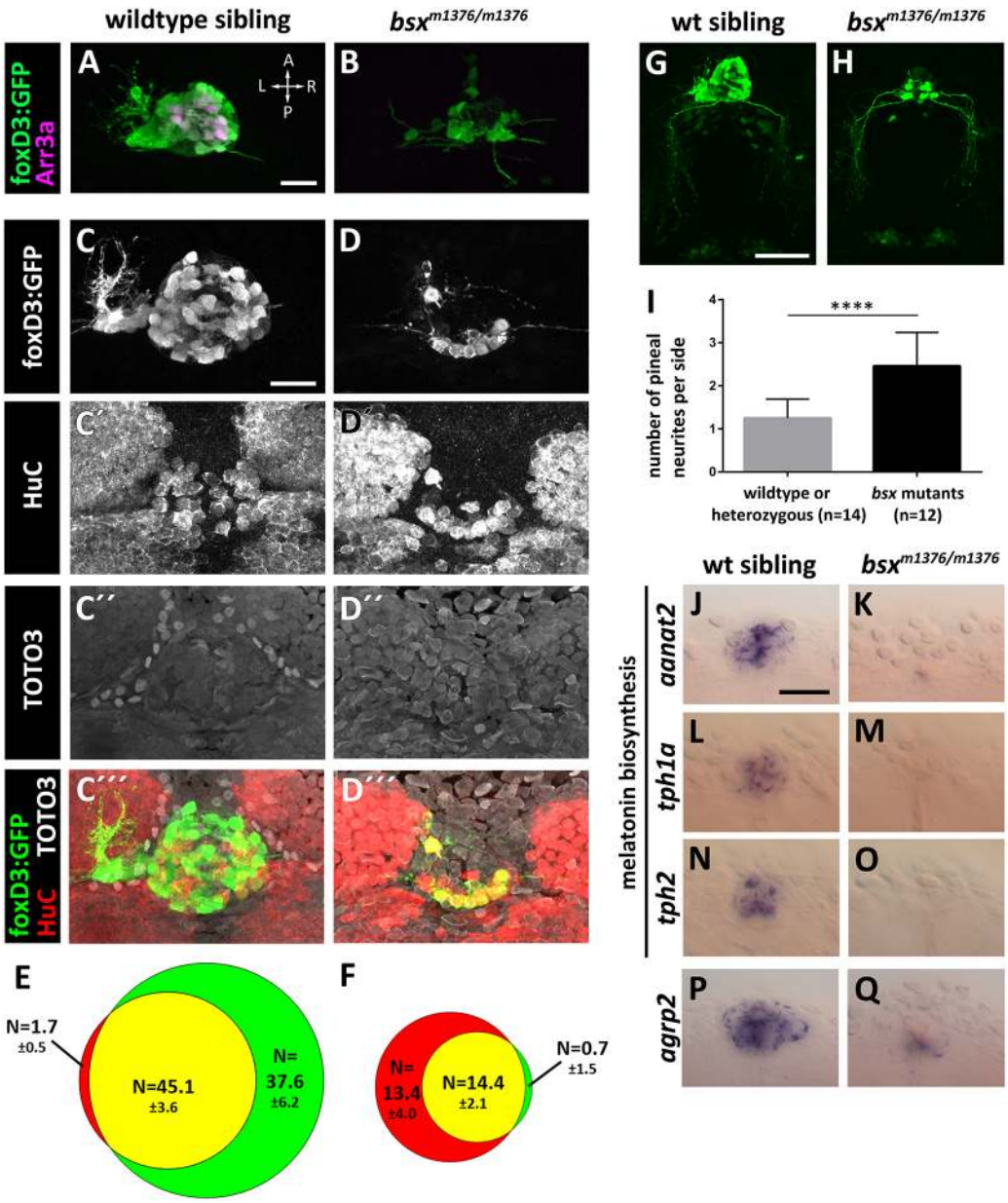

Fig. 6. Abnormal PC cell differentiation in *bsx* mutant embryos. (A,B) Immunofluorescence for GFP (labeling cone-like PhR cells and PNs) and Arr3a (labeling cone-like PhR cells) using *Tg(foxD3:GFP)* wild-type or *bsx* mutant embryos fixed at 78 hpf. Maximum-intensity projections. (C-D‴) Combined anti-HuC (labeling PNs) and anti-GFP immunofluorescence and TOTO3 nuclear staining of *Tg(foxD3:GFP)* wild-type or *bsx* mutant embryos fixed at 78 hpf. Images are maximum-intensity *z*-projections of 41 µm confocal stacks encompassing the PC (see Movie 1). (E,F) Average cell numbers±s.d. of GFP$^+$ (green), HuC$^+$ (red) and double-positive (yellow) cells of wild-type (E) and *bsx* mutant (F) embryos shown in C-D‴ (*n*=7 embryos). (G,H) Immunofluorescence for GFP using *Tg(foxD3:GFP)* wild-type or *bsx* mutant embryos fixed at 78 hpf. Maximum-intensity projections of confocal image stacks of PG cells and neurites originating from the PG are shown. (I) GFP$^+$ neurites of PNs in *Tg(foxD3:GFP) bsx* mutant or control embryos were counted. Graph shows average number of neurites per side (left or right hemisphere). Error bars indicate s.d. ****$P\leq0.0001$ as revealed by Wilcoxon–Mann–Whitney test. (J-Q) WISH expression analysis of genes encoding enzymes involved in melatonin biosynthesis (J-O) or Agrp2 neuropeptide (P,Q) in wild-type and *bsx* mutant embryos at 84 hpf (J,K) or 72 hpf (L-Q). Anterior is at the top of the images. All embryos were genotyped. (A,B,J-Q) $n\geq4$ embryos each for wild type and mutants. Scale bars: 20 µm (A-D‴) and 50 µm (G,H,J-Q).

Given that we demonstrated that Bsx acts on *otx5*, a well-established determinant of PhR cell fate, we tested whether the effects of Bsx loss on pineal PhR cells were secondary effects resulting from downregulation of *otx5*. Thus, we assessed *opn1sw1* expression in embryos injected with a MO against *otx5* (Gamse et al., 2002), but were unable to detect *opn1sw1* in the PG of those embryos at 2 dpf (Fig. S7L,M). By contrast, *bsx* mutant embryos expressed *opn1sw1* in the PG at 2 dpf (Fig. S5O,P), indicating that Bsx has a function in PhR cell differentiation that cannot solely be explained through the regulation of *otx5*. Given that Tbx2b specifically promotes UV-cone cell fate in the retina (Alvarez-Delfin et al., 2009), we assessed whether knock down of *tbx2b* would interfere with ectopic *opn1sw1* expression in *bsx* mutants. We found a significantly reduced pineal *opn1sw1* expression in *bsx* mutants upon knock down of *tbx2b* (Fig. S11). This was consistent with Tbx2b positively and Bsx negatively regulating *opn1sw1* expression.

The ambiguous effects of Bsx loss on cone- or rod-like marker gene expression raise doubts about cell type specificity in the

Development (2018) 145, dev163477. doi:10.1242/dev.163477

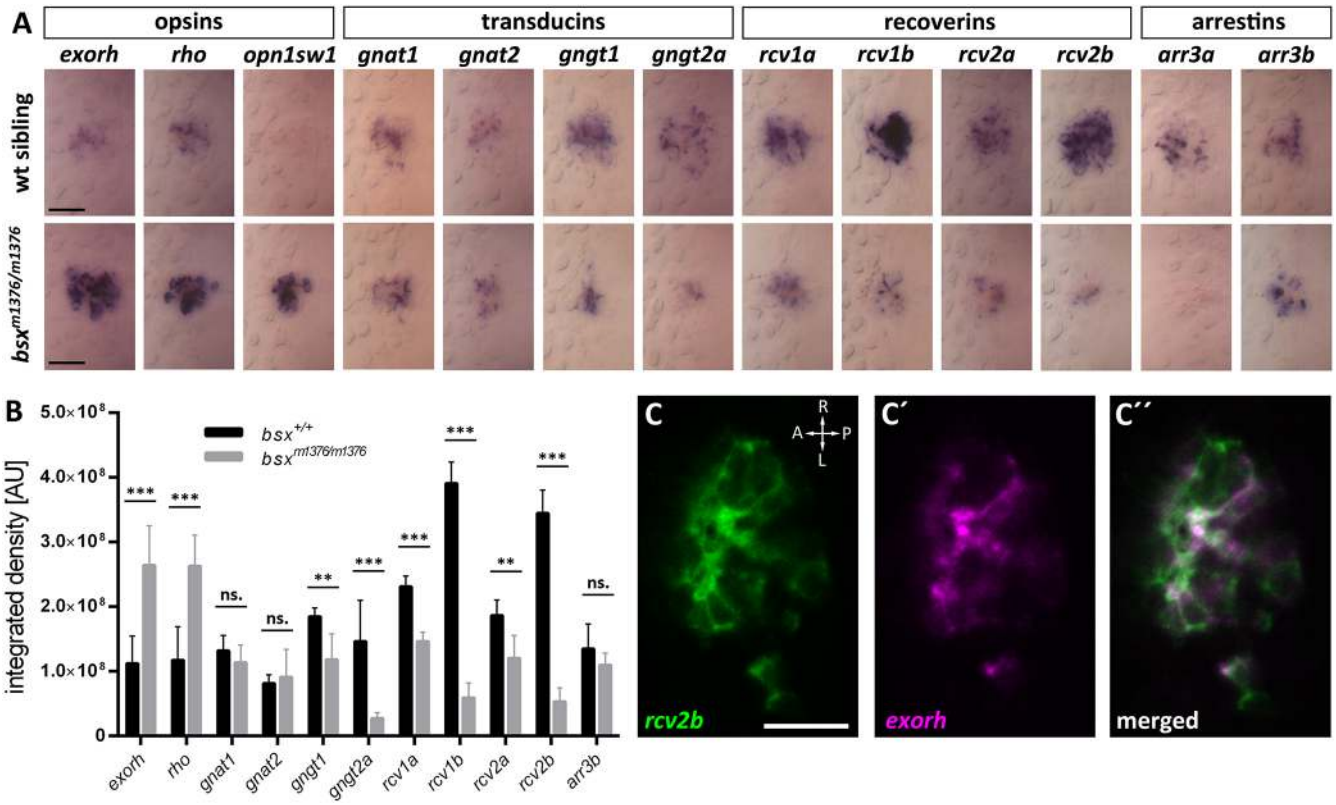

Fig. 7. Expression of genes encoding phototransduction factors is altered in *bsx* mutants. (A) Expression of phototransduction factor genes was analyzed by WISH in embryos at 78 hpf. Genotypes are indicated on the left and gene expression analyzed is indicated above the images. At the top, different biochemical classes of phototransduction factors are indicated. Anterior is to the left of each image. For each genotype and gene expression, *n*=7 embryos were analyzed. (B) For each individual stained embryo, stain density was measured and integrated over the PC region to evaluate changes in the number of cells expressing a marker or in expression level (method outline in Fig. S10). Significance was determined through Wilcoxon–Mann–Whitney test. $^{**}P \leq 0.01$; $^{***}P \leq 0.001$. ns, not significant. (C-C″) Single *z*-plane (1.5 µm) from confocal stack of wild-type PG (dorsal view) fixed 3 dpf and analyzed by double-fluorescent WISH for expression of *rcv2b* [(C) green], *exorh* [(C′) magenta]; (C″) shows merged channels. Orientations as indicated in (C). Scale bars: 30 µm (A) and 20 µm (C-C″).

zebrafish PC during early larval stages. Using double-fluorescent WISH, we visualized *exorh* and *rcv2b* transcripts, which selectively label rod or cone PhR cells, respectively. To our surprise, instead of a mutually exclusive expression pattern, we found colocalization of *exorh* and *rcv2b* transcripts in PG cells of wild-type larvae 78 hpf (Fig. 7C-C″). This suggests that, at the developmental stage analyzed, PG cells do not strictly segregate into cells expressing exclusively rod or cone markers.

DISCUSSION

Our study identifies the highly conserved Bsx homeodomain transcription factor as a major regulator of PC development in zebrafish, affecting specification of the pineal anlage, including the PP, cell lineage decisions, morphogenesis and differentiation in the pineal system (Fig. 8A). *bsx* expression starts in the pineal anlage around the 10-somite stage, and, thus, slightly later than that of *flh* and *tbx2b* (both at the 6-somite stage; Snelson et al., 2008b) or *nr2e3* (8-somite stage; Khuansuwan et al., 2016). In line with *flh* being expressed earlier than *bsx*, Flh contributes to activation of *bsx* expression, even though, in some pineal anlage cells, Flh is not strictly required for *bsx* to be expressed. Loss of Bsx activity in turn does not affect *flh* expression. Analysis of *flh* and *bsx* double-mutant embryos revealed that Flh and Bsx act in parallel in specification of the pineal anlage, because only double mutants lacked *otx5* expression completely, suggesting an absence of PhR cells. The transcription factor Flh can be grouped together with Bsx into the ANTP class of homeodomain proteins (Ferrier, 2016), and might share target specificity, providing a potential molecular basis for partial redundancy of both transcription factors.

Our data further suggest that, in the control of *flh* and *bsx* expression, two signaling pathways converge: Wnt and Bmp, which together pattern the dorsal diencephalon and specify the pineal anlage. Wnt signaling induces *flh* and determines the extent of the pineal anlage in the dorsal diencephalon (Masai et al., 1997). Surprisingly, despite the vast expansion of the *flh* domain upon ectopic Wnt signaling, we did not observe a concomitant expansion of the *bsx* expression domain in the dorsal diencephalon. By contrast, we found the *bsx* expression domains to be specified by Bmp signaling levels. Bmp was previously described in early dorsoventral patterning of the neural plate (Barth et al., 1999), as well as in later aspects of PG development, when it promotes PhR cell fate (Quillien et al., 2011). However, our data revealed that Bmp also has a role in pineal anlage specification shortly after neural tube closure. This supports a model in which Wnt and Bmp signaling provide the spatial coordinates to control Flh and Bsx activity, respectively. Given that Wnt activity has been reported to expand the pineal anlage anteriorly (Masai et al., 1997), whereas we see a Bmp-mediated expansion of the *bsx* domain in a ventral direction, we hypothesize that surface ectoderm-derived Bmp specifies the ventral extent of the pineal anlage, whereas Wnt signaling specifies the anterior extent.

The generation of pineal asymmetry crucially depends on Nodal signaling, which controls unilateral expression of *pitx2c* in the left diencephalon and PP development (Liang et al., 2000; Concha et al., 2000; Garric et al., 2014). Although Nodal is not required for *bsx*

Development (2018) 145, dev163477. doi:10.1242/dev.163477

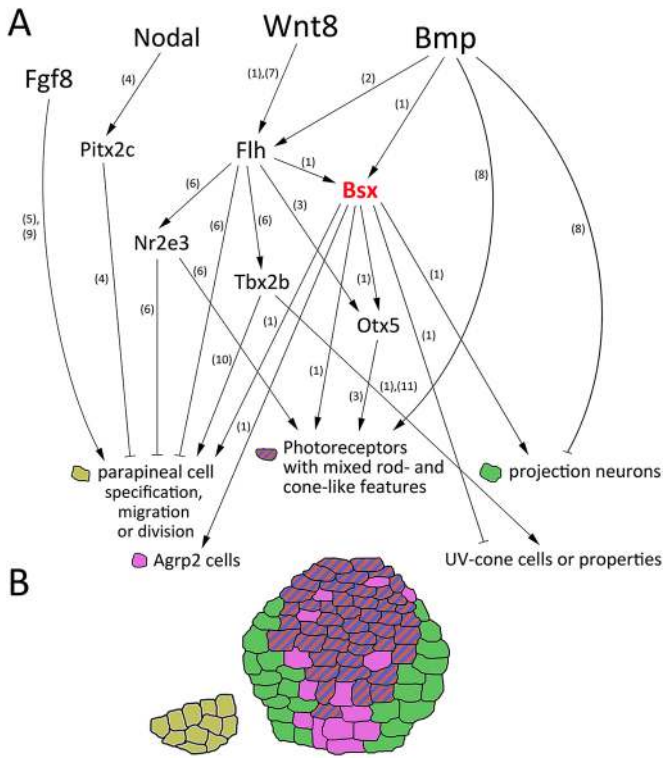

Fig. 8. Model positioning *bsx* in the regulatory network controlling PC development. (A) The model summarizes our findings on the epistatic position of *bsx* in the PC specification network and places them relative to previously characterized regulatory interactions. The model includes early signals involved in induction and patterning of the PC, as well as the transcription factor network that controls cell specification and differentiation. Arrows do not imply that interactions are direct. The regulation converges on the PC cell types indicated at the bottom of (A). For PP cells, effects of factors on specification, migration or differentiation are not distinguished here. References for specific regulatory interactions are indicated by numbers in parenthesis: (1) this study, (2) (Barth et al., 1999), (3) (Gamse et al., 2002), (4) (Garric et al., 2014), (5) (Regan et al., 2009), (6) (Khuansuwan et al., 2016), (7) (Masai et al., 1997), (8) (Quillien et al., 2011), (9) (Clanton et al., 2013), (10) (Snelson et al., 2008b) and (11) (Alvarez-Delfin et al., 2009). (B) Schematic representation of cell type diversity and distribution in the zebrafish PC at ~3-4 dpf. The dorsal view is shown, with the anterior at the top. Pineal PhR cells are depicted hatched in red and blue to indicate shared properties of cone-like and rod-like cells, respectively. PhR cells appear to cluster in the anterior half of the PG, whereas Agrp2 cells were preferentially detected in the posterior and medial regions, and PNs in the posterior and lateral regions of the PG.

expression in the pineal anlage, when we abolished Nodal asymmetry in *ntl/ta* mutants, sidedness of unilateral *bsx* expression in the PP primordium was randomized. Our loss-of-function experiments revealed that *bsx* and *pitx2c* expression do not regulate each other. However, we found a complete absence of the PP in *bsx* mutants, as judged by *otx5*, *gfi1ab*, *lhx2* and *sox1a* expression, revealing a strict requirement for *bsx* in PP development. *fgf8a* expression, which appears to instruct PP cell fate (Clanton et al., 2013) as well as PP cell migration away from the midline (Regan et al., 2009), is expressed normally in *bsx* mutants, as is *tbx2b*, which instructs PP formation (Snelson et al., 2008b). Thus, we conclude that Bsx is strictly required for PP cell specification in the pineal primordium. In line with the established role of the PP in development of habenular asymmetry (Gamse et al., 2003), the habenulae in *bsx* mutant embryos were right isomerized. Complex behavioral phenotypes of right-isomerized zebrafish recently received attention (Facchin et al., 2015), for which *bsx* mutant zebrafish could constitute a valuable genetic model.

Our analysis of confocal stacks of labeled cell types in the PG suggested that PG cell types are spatially clustered: although it is well established that PNs are located in lateral positions in the caudal two-thirds of the PG, our data suggest that PhR cells cluster in the rostral median PG (Fig. 8B). In *bsx* mutants, this organization was disturbed, and the PNs clustered at the caudal margin of the PG, suggesting that Bsx is also required for proper spatial organization of different cell types.

Our data further revealed that Bsx controls cell differentiation of multiple cell types in the PG. Melatonin is a prominent PG neuroendocrine hormone with circadian expression in zebrafish (Gothilf et al., 1999). Different from circadian *bsx* expression reported in *Xenopus* larval PGs (D'Autilia et al., 2010), we could not detect circadian modulation of *bsx* expression in the zebrafish PG. However, *bsx* mutant PGs did not express *tph1a*, *tph2* or *aanat2*, and, thus, are devoid of serotonin- and melatonin-producing PG cells. Loss of melatonin was recently reported to disturb sleep patterns in zebrafish (Gandhi et al., 2015), and *bsx* mutants could provide a model to assess melatonin and potential pineal-specific serotonin functions. Furthermore, we found Bsx to regulate *agrp2* expression in the PC, suggesting that these *bsx*-expressing cell lineages might share Bsx transcriptional targets with hypothalamic cell lineages in which BSX regulates expression of the orexigenic neuropeptide Agrp (Sakkou et al., 2007).

The severe effects of loss of Bsx on cell lineages were also reflected by a more than fivefold reduction in GFP-expressing cells in *Tg(foxd3:GFP)*, as well as a reduction in HuC^{+} PN numbers by approximately half. Although the remaining PNs did form neurites, these projections showed aberrant branching morphology compared with wild-type embryos. We do not know the cause for the projection phenotype, but the abnormal caudomedial clustering of PNs in *bsx* mutants could lead to different neurite exit points from the PG and different axon navigation environments.

Rod-, red/green- and blue cone-specific opsins have been reported for the teleost PG (Ekström and Meissl, 2003). However, it remains unclear whether this corresponds to different PhR cell types or to a single cell type with mixed PhR properties. We found a putative rod-specific marker (*gngT1*) to be downregulated in *bsx* mutants, whereas others (*rho* and *exorh*) were upregulated. Similarly, we found several supposedly cone-specific markers (*gngT2a*, *rcv1b*, *rcv2a* and *rcv2b*) to be downregulated in *bsx* mutants, whereas, strikingly, the cone-specific UV-sensitive opsin *opn1sw1* was strongly expressed in *bsx* mutant but not wild-type embryos. In terms of spectral sensitivity, we could not find a clear tendency of Bsx influencing short-wave- or longer-wave-specific PhR cells. However, when we arranged the PhR cell markers according to their functional role in the phototransduction cascade, we detected a pattern consistent with a role of Bsx or its downstream effectors in downregulating opsin expression, but promoting expression of recoverins, as well as of specific transducins and *arr3a*. Thus, we hypothesize that Bsx in PhR cell differentiation is involved in regulatory circuits encoding PhR cell compensation strategies, balancing the relative expression of photopigments and downstream components of the phototransduction cascade. In line with this hypothesis, we assume abnormalities in response kinetics and light adaptation of pineal PhR cells in *bsx* mutants.

The observation that rod- or cone-like markers were affected differentially in *bsx* mutants prompted us to test the identity of pineal PhR cells. We found cells in which expression of the rod-specific *exorh* was colocalized with cone-specific *rcv2b*. If co-expression of these and other markers are confirmed in future studies, the current model of clearly distinct cone-like and rod-like PhR cells in the larval

Development (2018) 145, dev163477. doi:10.1242/dev.163477

PG needs to be re-examined. Although morphologically it is difficult to classify pineal PhR cells according to a canonical rod/cone discrimination, two clearly distinct types of PhR cells can be detected in the adult teleost PG based on electrophysiological properties (Ekström and Meissl, 2003). Therefore, co-expression in the embryo could be a transient phenomenon and correspond to PhR progenitor cells with the plasticity to develop into cone- or rod-like PhR cells during postembryonic stages. The idea of cone-to-rod and rod-to-cone 'transmutations' was proposed more than 80 years ago (Walls, 1934), and was recently supported by findings in snakes (Schott et al., 2016; Simões et al., 2016). Thus, early developmental plasticity could contribute to evolutionary dynamics.

Bsx has crucial roles in distinct steps of PC development, including early PC specification, PP formation and PhR cell differentiation. These roles might be conserved, in part, in neuroendocrine mammalian pinealocytes, notwithstanding their loss of photoreceptive functions. Furthermore, Bsx in the PC is crucial for asymmetric differentiation of the zebrafish habenulae, structures for which asymmetries were recently demonstrated both in volume (Ahumada-Galleguillos et al., 2017) and connectivity (Hétu et al., 2016) also in humans. Thus, *bsx* mutant zebrafish could be developed as a model to study fundamental questions in neurobiology, including brain asymmetry, circuits balancing expression of photopigment and phototransduction components, and brain function without melatonin and pineal serotonin.

MATERIALS AND METHODS

Zebrafish strains, maintenance and heat shock treatment

Zebrafish embryos were obtained through natural breeding of ABTL zebrafish. All embryos were kept in 3 g/l Red Sea salt (Red Sea) and 28.5°C under standard conditions in a 14 h light/10 h dark cycle and staged according to Kimmel et al. (1995). To prevent pigmentation, embryos were treated with 0.2 mM *N*-phenylthiourea (Sigma-Aldrich).

The following mutant or transgenic lines were used: *bsx*^{m1376} (this study), *ntl*^{b160} (Halpern et al., 1993), *flh*^{n1} (Talbot et al., 1995), *ace/fgf8a*^{ti282a} (Reifers et al., 1998), *Tg(foxD3:GFP)*^{zf15} (Gilmour et al., 2002), *Tg(hsp70l:Bmp2b)*^{fr13} (Chocron et al., 2007), *Tg(hsp70l:dnXlaBmpr1a-GFP)*^{w30} (Pyati et al., 2005) and *Tg(hsp70l:Wnt8a-GFP)*^{w34} (Weidinger et al., 2005).

All experiments were carried out in accordance with the German Animal Welfare Act.

Heat shock was performed by placing petri dishes with zebrafish embryos in a 39°C water bath for 1 h.

Cloning

For cDNA cloning, total RNA was extracted from embryos of the desired staged, homogenized using a syringe (100 Sterican, Ø 0.60×30 mm, Braun), and suspended in 600 µl RLT Lysis Buffer from the RNAeasy Mini Kit (Qiagen), complemented with 10 µl 2-mercaptoethanol. Lysate was then filtered on a QIAshredder column (Qiagen) before RNA extraction was continued using the RNAeasy Mini Kit (Qiagen) following the manufacturer's protocol. Total RNA was then used as template for cDNA synthesis using random primers and the Superscript III RT-PCR system (Thermo Fisher Scientific). Coding-sequence fragments were PCR amplified from cDNA using MyTaq DNA Polymerase (Bioline). Amplicons were analyzed on standard gel electrophoresis for correct size and then subcloned into pCRII-TOPO (Invitrogen). All the primer sequences used are shown in Table S1. Correct insertions into vector backbone were confirmed by sequencing. For all plasmids used as template for *in vitro* transcription of antisense RNA probes, see Table S2.

The full-length wild-type *bsx* coding sequence was amplified from cDNA using the primers shown for *bsx* in Table S1. For Gateway cloning, the forward primer (annealing part in italic) was flanked with an attB1 site (bold): 5′-**GGGGACAAGTTTGTACAAAAAAGCAGGCT**TGAT*ATG-AATCTGAACTACACGTCTCCG*-3′. The reverse primer (annealing part in italic) was flanked with an attB2R site (bold): 5′-**GGGGACCACTTTG-TACAAGAAAGCTGGGT**CTA*CTAGAGTAAATGTTCAGGAGAGCAA*-3′. A BP recombination reaction was performed using the Gateway BP Clonase II Enzyme Mix (Thermo Fisher Scientific) to generate the Gateway middle entry plasmid pME-*bsx*. pME-*bsx* was then recombined in a Multisite Gateway 4-1-2-3 reaction using LR Clonase II Plus Enzyme (Thermo Fisher Scientific) together with the following three plasmids: p5E-CMV/SP6, p3E-polyA and pDestTol2pA2 (all from the Tol2Kit, Kwan et al., 2007) to generate a CMV/SP6:*bsx*-polyA-pDest construct. Full-length *m1376 bsx* mRNA was amplified from cDNA of embryos resulting from a *bsx*$^{+/m1376}$ in-cross using the primers shown for *bsx* in Table S1 and subcloned into pCRII-TOPO (Invitrogen). The *bsx*^{m1376} fragment was excised from an identified clone using *Xho*I and *Spe*I and subcloned into a pCS2+ vector opened with *Xho*I and *Xba*I to generate a *bsx*^{m1376}-pCS2+ construct. Sequencing revealed no or only silent mutations (potential polymorphisms) within the reading frame of wild-type *bsx* and *bsx*^{m1376}, which harbors the TALEN-induced mutation.

Mutagenesis and genotyping

bsx TALEN mRNA was transcribed from TAL3034 (Addgene plasmid #41208, deposited by Keith Joung) and TAL3035 (Addgene plasmid #41209, deposited by Keith Joung) (Sander et al., 2011). Then, 1 µg of *Age*I-linearized plasmids were used as a template for mRNA transcription with the mMessage mMachine T7 Transcription kit (Ambion/Thermo Fisher Scientific). Fertilized ABTL eggs were injected with *bsx* TALEN mRNA (200 pg each, for left and right TALEN, per embryo). Twelve injected embryos at 24 hpf were pooled and lysed in Lysis Buffer (10 mM Tris-HCl pH 8, 30 mM KCl, 30 mM NaCl, 1 mM EDTA, 0.5% Tween20, 0.5% Nonidet P-40) containing 1 mg/ml Proteinase K (Sigma-Aldrich). *Xho*I (NEB) digest of a PCR fragment covering the TALEN target region (forward: 5′-ATTGCAA-AAGGAATGCAGATG-3′; reverse: 5′-ATTGTCGTCCAGCGTGTATCT-3′; Fig. S1B) confirmed the occurrence of indels disrupting the *Xho*I recognition site. Genotyping of further generations was performed using the same PCR and X*ho*I digest after lysing fin clips or embryonic tails in 50 mM NaOH for 45 min at 95°C, then neutralizing lysis with 1/10 volume 1 M Tris-HCl pH 7.5, before 2 µl of lysed tissue were used for PCR. Then, 15 µl of the PCR reaction was used for *Xho*I digest and restriction-length polymorphism was visualized by agarose gel electrophoresis (Fig. S1C).

Morpholino and mRNA injections

All MOs used in this study have previously been described and were ordered from Gene Tools. MOs were diluted in water and a volume of 1-2 nl was injected into the yolk of embryos at the one-cell stage. For details, see Table 1. Control embryos were injected with 1-2 nl of standard control MO (5′-CCTCTTACCTCAGTTACAATTTATA-3′).

Functional knock down of Otx5 was confirmed by downregulation of *irbp* in the PG (Gamse et al., 2002, Fig. S5C,D). Splice-blocking activity of the *nr2e3* MO was confirmed by RT-PCR on 24 hpf total RNA, revealing the presence of a 300 bp band in knockdown embryos as opposed to a 210 bp band in controls (Fig. S7I) when using the following primers on cDNA: 5′-GGACTTCTTTGTAAAGTGTGTTCTGAC-3′ and 5′-TCATT-CCAGCTTGAAGGCATTTC-3′. Functional knock down of Tbx2b was confirmed by absence of the PP cell cluster in the majority of injected embryos (Fig. S7F).

lefty1 (zf-lefty1-pCS2+; Thisse and Thisse, 1999), *gfp* (pG1-GFP; gift from Gudrun Aspöck) and *bsx*^{m1376} mRNA (*bsx*^{m1376}-pCS2+, this study) were synthesized from *Not*I (NEB) linearized plasmids, and wild-type *bsx* mRNA (CMV/SP6:*bsx*-polyA-pDest, this study) from a *Kpn*I (NEB) linearized plasmid, using the Ambion mMessage mMachine Transcription kit, T7 or SP6, according to the manufacturer's protocol.

Whole-mount *in situ* hybridization and apoptosis assay

WISH was carried out as described (Thisse et al., 1993) with the following modifications. Digoxigenin (DIG)-labeled RNA antisense probes were transcribed from the plasmids in Table S2 using T7, SP6 or T3 RNA polymerase (Thermo Scientific Scientific) following the manufacturer's protocol, and were used full length (without alkaline hydrolysis). After dehydration, embryos were subjected to Proteinase K (10 µg/ml in PBST) digestion at room temperature: 3 min for 16 hpf, 5 min for 20 hpf, 10 min for 24 hpf, 15 min for 30 hpf, 25 min for 2 dpf, 45 min for 3 dpf, and 60 min

Development (2018) 145, dev163477. doi:10.1242/dev.163477

Table 1. MOs used in this study

Target gene	Sequence	Type	Concentration	Reference
nr2e3	5′-ATACGCAAGTTGTTTTCTCACCTGT-3′	Splice blocking	6 ng/µl	(Khuansuwan et al., 2016)
otx5	5′-CATGACTAAACTCTCTCTCTCTCTC-3′	ATG-blocking	1 ng/µl	(Gamse et al., 2002)
pitx2c	5′-GATCCTTCATAGAGGTCATGGATAA-3′	ATG-blocking	6 ng/µl	(Garric et al., 2014)
tbx2b	5′-AAAATATGGGTACATACCTTGTCGT-3′	Splice blocking	6 ng/µl	(Gross and Dowling, 2005)

for 4 dpf embryos. The embryos were then post-fixed in 4% PFA/PBST for 30 min. PFA was washed out five times for 5 min in PBST, and embryos were prehybridized in Hybridization Mix [5 mg/ml *Torula* RNA (Sigma-Aldrich), 50 µg/ml heparin (Sigma-Aldrich), 0.1% Tween 20 (AppliChem) in 50% formamide (AppliChem)/5× SSC] for at least 2 h at 65°C, then incubated overnight in Hybridization Mix containing the probe. The following day, embryos were washed for 20 min each at 65°C: twice in 50% formamide/2× SSCT, twice in 25% formamide/2× SSCT, twice in 2× SSCT, and twice in 0.2× SSCT. They were transferred to PBST and washed twice in PBST at room temperature (5 min each). Embryos were blocked for at least 2 h at room temperature in Blocking Solution [2 mg/ml BSA (AppliChem), 5% sheep serum, in PBST], and incubated with anti-DIG-AP Fab Fragments (Roche) 1:4000 overnight at 4°C. Embryos were then washed six times for 20 min each in PBST and three times for 10 min each in NTMT [0.1 M Tris-HCl (pH 9.5), 0.1 M NaCl, 0.05 M $MgCl_2$, 0.1% Tween 20]. Staining reaction was in NTMT containing NBT (45 µg/ml) and BCIP (20 µg/ml). After staining, embryos were rinsed in 1 mM EDTA/PBST and post-fixed in 4% PFA for 1 h or overnight at 4°C. Then, embryos were rinsed again in PBST and transferred to 1 mM EDTA/80% glycerol/20% PBST for storage and documentation.

Double-fluorescent WISH was carried out as previously described (Ronneberger et al., 2012).

Apoptotic cells were visualized through a TUNEL assay using the ApopTag peroxidase *in situ* apoptosis-detection kit (Merck S7100), as previously described (Ryu et al., 2005).

Integrated density measurement of WISH signals

To quantify signals after WISH, *z*-stack images were recorded of embryos with low differential interference contrast (DIC) contrast settings. Minimum intensity projections of 25 *z*-planes (1 µm each) encompassing the PG were made with ImageJ. These pictures were then converted to 8-bit gray-scale and inverted. Integrated Density was then calculated for an area surrounding the PG (80 µm circle for Fig. 7 and Fig. S10) or the whole PC (80 µm×120 µm for Fig. S2), and a larger area surrounding the PC (100 µm diameter or 96 µm×138 µm). A threshold value was determined by dividing the area difference by the Integrated Density difference and the picture histogram was clipped at the lower end to this threshold value. After this background subtraction, the Integrated Density of the smaller area was calculated from the adjusted picture (see also Fig. S10 for the described workflow), and is shown in bar or line charts (Figs 7, S2 and S11).

Immunohistochemistry

Immunohistochemistry was performed as previously described (Ronneberger et al., 2012). The following primary antibodies were used: rabbit anti-GFP polyclonal (Thermo Fisher Scientific, #A-1112, 1:1000 dilution), chicken anti-GFP polyclonal (Thermo Fisher Scientific, #A-10262, 1:1000 dilution), mouse anti-GFP monoclonal (Thermo Fisher Scientific, #A-11120, 1:1000 dilution), mouse anti-GFP monoclonal Living Colors Jl-8 (ClonTech/Takara Bio USA, Inc, #632381, 1:1000 dilution), Arrestin3a/zpr-1/Fret43 (Larison and Bremiller, 1990, ZIRC, ZFIN ID: ZDB-ATB-081002-43, 1:2 dilution of predilution) and HuC/HuD monoclonal (16A11, Thermo Fisher Scientific, #A-21271, 1:1000 dilution). As secondary antibodies, we used goat anti-rabbit IgG Alexa 488 (Thermo Fisher Scientific, #A-11070, 1:1000 dilution), goat anti-rabbit IgG Alexa 546 (Thermo Fisher Scientific, #A-11035, 1:1000 dilution), goat anti-chicken IgY Alexa 488 (Thermo Fisher Scientific, #A-11039, 1:1000 dilution), goat anti-chicken IgY Alexa 555 (Thermo Fisher Scientific, #A-21437, 1:1000 dilution), goat anti-mouse IgG Alexa 488 (#A-11001, 1:1000 dilution) and F(ab′)2-goat anti-mouse IgG Alexa 555 (Thermo Fisher Scientific, #A-21425, 1:1000 dilution). For nuclear staining, embryos after immunohistochemistry were incubated in TOTO-3 iodide (Invitrogen, 1:1000 dilution) overnight at 4°C, then washed in PBST and transferred to 80% glycerol/PBST for imaging.

Imaging and figure preparation

After standard DIG/alkaline phosphatase-based WISH, embryos were mounted for brightfield microscopy in 80% glycerol, 20% PBST, 1 mM EDTA. Pictures were taken with AxioCam CC1 on an AxioPlan2 microscope with a PLAN-NEOFLUAR 20×/0.5 or 10×/0.3 objective and DIC optics using the AxioVs40 Software (all Zeiss). From image stacks (1 µm step size), minimum intensity projections of all *z*-planes encompassing the PG were made using ImageJ.

Time-lapse imaging of *Tg(foxD3:GFP)*^{zf15} embryos was made using Examiner.D1 and ZEN blue software (all Zeiss). Embryos after fluorescent WISH and immunohistochemistry were recorded using a Zeiss LSM 510 or LSM 880. All figures were assembled using Adobe Photoshop CS4 or CS6. When linear adjustment of levels was made, histograms were clipped to the same values for experimental and control images.

Chemical treatment

To treat embryos with the Wnt inhibitor IWR-1 (Sigma-Aldrich), 75 µl of a 2 mM IWR-1/DMSO stock solution or DMSO alone was added to 30 ml of E3 medium. Embryos were then kept in this 5 µM IWR-1 working concentration or 0.25% DMSO as control starting from 2 hpf until fixed for analysis.

Data analysis and statistics

All charts in this manuscript were generated using GraphPad Prism 6 with the following exceptions: line chart in Fig. S2 (MS Excel 2016), bar chart in Fig. S5 (MS Excel 2016), Venn diagrams in Fig. 6 (Venn Diagram Plotter, PNNL, Apache License 2.0, https://omics.pnl.gov/software/venn-diagram-plotter). Sample sizes used in this study did not allow sensible testing for normal distribution. Thus, for pairwise comparison of two groups, we used the distribution-independent Wilcoxon–Mann–Whitney test, calculated with GraphPad Prism 6. Statistical significance is indicated as follows: $*P \leq 0.05$; $**P \leq 0.01$; $***P \leq 0.001$; $****P \leq 0.0001$; ns=not significant. If applicable, exact *P*-values and sample sizes (*n*) are given. For the experiment shown in Fig. S5, embryos from four groups were assigned to three phenotypic classes. We generated contingency tables and tested whether all values met the minimum expectation requirements for a chi-square goodness of fit test introduced by Yarnold in 1970, who proposed in a contingency table of three or more classes *s*, the minimum expectation can be as small as *5r/s*, with *r* denoting the number of expectations less than five (Yarnold, 1970). Applying this rule, we determined a minimum expectation of 3.33 and found all values in our contingency table to be above 3.33. Thus, we applied chi-square goodness of fit test using GraphPad Prism 6 to determine the *P*-values given in the legend of Fig. S5.

Acknowledgements

Thanks to Keith Joung for providing the *bsx* TALEN plasmids, Martha Manoli for cloning the *bsx* plasmid used for probe synthesis, Jochen Holzschuh for cloning the *tph2* plasmid used for probe synthesis, and Nadja Bischoff, Jana Ernesti, Lena Tittel and Janna Becker for technical assistance with genotyping. Many thanks to Sabine Götter for excellent fish care, Simone Königsmann and Daniela Reuter-Schmitt for technical assistance, and Logan Doil for proof-reading of the manuscript. Thanks to Heiko Löhr and Mathias Hammerschmidt for critical discussions and providing *Tg(hsp70l:Bmp2b)* zebrafish. Thanks to Wiebke Herzog for providing *flh* mutant zebrafish. Thanks to Yoav Gothilf for providing the *aanat2* plasmid for probe synthesis.

Competing interests
The authors declare no competing or financial interests.

Author contributions
Conceptualization: T.S., W.D.; Methodology: T.S., W.D.; Validation: T.S.; Formal analysis: T.S., W.D.; Investigation: T.S.; Resources: T.S.; Writing - original draft: T.S., W.D.; Writing - review & editing: T.S., W.D.; Visualization: T.S., W.D.; Supervision: W.D.; Project administration: W.D.; Funding acquisition: W.D.

Funding
This study was supported by the German Research Foundation (Deutsche Forschungsgemeinschaft, DFG) (grant EXC 294) BIOSS - Centre for Biological Signalling Studies (to W.D.).

Supplementary information
Supplementary information available online at
http://dev.biologists.org/lookup/doi/10.1242/dev.163477.supplemental

References

Ahumada-Galleguillos, P., Lemus, C. G., Díaz, E., Osorio-Reich, M., Härtel, S. and Concha, M. L. (2017). Directional asymmetry in the volume of the human habenula. *Brain Struct. Funct.* **222**, 1087-1092.

Akhmedov, N. B., Piriev, N. I., Chang, B., Rapoport, A. L., Hawes, N. L., Nishina, P. M., Nusinowitz, S., Heckenlively, J. R., Roderick, T. H., Kozak, C. A. et al. (2000). A deletion in a photoreceptor-specific nuclear receptor mRNA causes retinal degeneration in the rd7 mouse. *Proc. Natl. Acad. Sci. USA* **97**, 5551-5556.

Alvarez-Delfin, K., Morris, A. C., Snelson, C. D., Gamse, J. T., Gupta, T., Marlow, F. L., Mullins, M. C., Burgess, H. A., Granato, M. and Fadool, J. M. (2009). Tbx2b is required for ultraviolet photoreceptor cell specification during zebrafish retinal development. *Proc. Natl. Acad. Sci. USA* **106**, 2023-2028.

Barth, K. A., Kishimoto, Y., Rohr, K. B., Seydler, C., Schulte-Merker, S. and Wilson, S. W. (1999). Bmp activity establishes a gradient of positional information throughout the entire neural plate. *Development* **126**, 4977-4987.

Cau, E., Quillien, A. and Blader, P. (2008). Notch resolves mixed neural identities in the zebrafish epiphysis. *Development* **135**, 2681.

Chocron, S., Verhoeven, M. C., Rentzsch, F., Hammerschmidt, M. and Bakkers, J. (2007). Zebrafish Bmp4 regulates left-right asymmetry at two distinct developmental time points. *Dev. Biol.* **305**, 577-588.

Clanton, J. A. (2013). Fgf Signaling Governs the Differentiation of Parapineal Neurons in Zebrafish. *PhD thesis*, Vanderbilt University, Nashville, Tennessee.

Clanton, J. A., Hope, K. D. and Gamse, J. T. (2013). Fgf signaling governs cell fate in the zebrafish pineal complex. *Development* **140**, 323-332.

Concha, M. L. and Wilson, S. W. (2001). Asymmetry in the epithalamus of vertebrates. *J. Anat.* **199**, 63-84.

Concha, M. L., Burdine, R. D., Russell, C., Schier, A. F. and Wilson, S. W. (2000). A nodal signaling pathway regulates the laterality of neuroanatomical asymmetries in the Zebrafish forebrain. *Neuron* **28**, 399-409.

Cremona, M., Colombo, E., Andreazzoli, M., Cossu, G. and Broccoli, V. (2004). Bsx, an evolutionary conserved Brain Specific homeoboX gene expressed in the septum, epiphysis, mammillary bodies and arcuate nucleus. *Gene Expr. Patterns* **4**, 47-51.

D'Autilia, S., Broccoli, V., Barsacchi, G. and Andreazzoli, M. (2010). Xenopus Bsx links daily cell cycle rhythms and pineal photoreceptor fate. *Proc. Natl. Acad. Sci. USA* **107**, 6352-6357.

Dodt, E. (1973). The parietal eye (pineal and parietal organs) of lower vertebrates. In *Visual Centers in the Brain - Handbook of Sensory Physiology*, Vol. 7 (ed. H. Autrum), pp. 113-140. Berlin, Heidelberg: Springer Berlin Heidelberg.

Duboc, V., Dufourcq, P., Blader, P. and Roussigné, M. (2015). Asymmetry of the Brain: development and Implications. *Annu. Rev. Genet.* **49**, 647-672.

Ekström, P. and Meissl, H. (2003). Evolution of photosensory pineal organs in new light: the fate of neuroendocrine photoreceptors. *Philos. Trans. R. Soc. Lond. B Biol. Sci.* **358**, 1679-1700.

Facchin, L., Duboué, E. R. and Halpern, M. E. (2015). Disruption of epithalamic left-right asymmetry increases anxiety in Zebrafish. *J. Neurosci.* **35**, 15847-15859.

Ferrier, D. E. K. (2016). Evolution of homeobox gene clusters in animals: the giga-cluster and primary vs. secondary clustering. *Front. Ecol. Evol.* **4**, 366.

Gamse, J. T., Shen, Y.-C., Thisse, C., Thisse, B., Raymond, P. A., Halpern, M. E. and Liang, J. O. (2002). Otx5 regulates genes that show circadian expression in the zebrafish pineal complex. *Nat. Genet.* **30**, 117-121.

Gamse, J. T., Thisse, C., Thisse, B. and Halpern, M. E. (2003). The parapineal mediates left-right asymmetry in the zebrafish diencephalon. *Development* **130**, 1059-1068.

Gandhi, A. V., Mosser, E. A., Oikonomou, G. and Prober, D. A. (2015). Melatonin is required for the circadian regulation of sleep. *Neuron* **85**, 1193-1199.

Garric, L., Ronsin, B., Roussigné, M., Booton, S., Gamse, J. T., Dufourcq, P. and Blader, P. (2014). Pitx2c ensures habenular asymmetry by restricting parapineal cell number. *Development* **141**, 1572-1579.

Gilmour, D. T., Maischein, H.-M. and Nüsslein-Volhard, C. (2002). Migration and function of a glial subtype in the vertebrate peripheral nervous system. *Neuron* **34**, 577-588.

Gordon, P. J., Yun, S., Clark, A. M., Monuki, E. S., Murtaugh, L. C. and Levine, E. M. (2013). Lhx2 balances progenitor maintenance with neurogenic output and promotes competence state progression in the developing retina. *J. Neurosci.* **33**, 12197-12207.

Gothilf, Y., Coon, S. L., Toyama, R., Chitnis, A., Namboodiri, M. A. A. and Klein, D. C. (1999). Zebrafish serotonin N-acetyltransferase-2: marker for development of pineal photoreceptors and circadian clock function. *Endocrinology* **140**, 4895-4903.

Gross, J. M. and Dowling, J. E. (2005). Tbx2b is essential for neuronal differentiation along the dorsal/ventral axis of the zebrafish retina. *Proc. Natl. Acad. Sci. USA* **102**, 4371-4376.

Halpern, M. E., Ho, R. K., Walker, C. and Kimmel, C. B. (1993). Induction of muscle pioneers and floor plate is distinguished by the zebrafish no tail mutation. *Cell* **75**, 99-111.

Hétu, S., Luo, Y., Saez, I., D'Ardenne, K., Lohrenz, T. and Montague, P. R. (2016). Asymmetry in functional connectivity of the human habenula revealed by high-resolution cardiac-gated resting state imaging. *Hum. Brain Mapp.* **37**, 2602-2615.

Hong, E., Santhakumar, K., Akitake, C. A., Ahn, S. J., Thisse, C., Thisse, B., Wyart, C., Mangin, J.-M. and Halpern, M. E. (2013). Cholinergic left-right asymmetry in the habenulo-interpeduncular pathway. *Proc. Natl. Acad. Sci. USA* **110**, 21171-21176.

Khuansuwan, S. and Gamse, J. T. (2014). Identification of differentially expressed genes during development of the zebrafish pineal complex using RNA sequencing. *Dev. Biol.* **395**, 144-153.

Khuansuwan, S., Clanton, J. A., Dean, B. J., Patton, J. G. and Gamse, J. T. (2016). A transcription factor network controls cell migration and fate decisions in the developing zebrafish pineal complex. *Development* **143**, 2641-2650.

Kimmel, C. B., Ballard, W. W., Kimmel, S. R., Ullmann, B. and Schilling, T. F. (1995). Stages of embryonic development of the zebrafish. *Dev. Dyn.* **203**, 253-310.

Kwan, K. M., Fujimoto, E., Grabher, C., Mangum, B. D., Hardy, M. E., Campbell, D. S., Parant, J. M., Yost, H. J., Kanki, J. P. and Chien, C.-B. (2007). The Tol2kit: a multisite gateway-based construction kit for Tol2 transposon transgenesis constructs. *Dev. Dyn.* **236**, 3088-3099.

Lagman, D., Callado-Pérez, A., Franzén, I. E., Larhammar, D. and Abalo, X. M. (2015). Transducin duplicates in the Zebrafish retina and pineal complex: differential specialisation after the teleost tetraploidisation. *PLoS ONE* **10**, e0121330.

Larison, K. D. and Bremiller, R. (1990). Early onset of phenotype and cell patterning in the embryonic zebrafish retina. *Development* **109**, 567-576.

Liang, J. O., Etheridge, A., Hantsoo, L., Rubinstein, A. L., Nowak, S. J., Izpisúa Belmonte, J. C. and Halpern, M. E. (2000). Asymmetric nodal signaling in the zebrafish diencephalon positions the pineal organ. *Development* **127**, 5101-5112.

Masai, I., Heisenberg, C.-P., Barth, K. A., Macdonald, R., Adamek, S. and Wilson, S. W. (1997). floating head and masterblind regulate neuronal patterning in the roof of the forebrain. *Neuron* **18**, 43-57.

McArthur, T. and Ohtoshi, A. (2007). A brain-specific homeobox gene, Bsx, is essential for proper postnatal growth and nursing. *Mol. Cell. Biol.* **27**, 5120-5127.

Meissl, H. and Yáñez, J. (1994). Pineal photosensitivity. A comparison with retinal photoreception. *Acta Neurobiol. Exp. (Wars)* **54** Suppl., 19-29.

Pyati, U. J., Webb, A. E. and Kimelman, D. (2005). Transgenic zebrafish reveal stage-specific roles for Bmp signaling in ventral and posterior mesoderm development. *Development* **132**, 2333-2343.

Quillien, A., Blanco-Sanchez, B., Halluin, C., Moore, J. C., Lawson, N. D., Blader, P. and Cau, E. (2011). BMP signaling orchestrates photoreceptor specification in the zebrafish pineal gland in collaboration with Notch. *Development* **138**, 2293-2302.

Regan, J. C., Concha, M. L., Roussigne, M., Russell, C. and Wilson, S. W. (2009). An Fgf8-dependent bistable cell migratory event establishes CNS asymmetry. *Neuron* **61**, 27-34.

Reifers, F., Böhli, H., Walsh, E. C., Crossley, P. H., Stainier, D. Y. and Brand, M. (1998). Fgf8 is mutated in zebrafish acerebellar (ace) mutants and is required for maintenance of midbrain-hindbrain boundary development and somitogenesis. *Development* **125**, 2381-2395.

Renninger, S. L., Gesemann, M. and Neuhauss, S. C. F. (2011). Cone arrestin confers cone vision of high temporal resolution in zebrafish larvae. *Eur. J. Neurosci.* **33**, 658-667.

Roberson, S. and Halpern, M. E. (2018). Development and connectivity of the habenular nuclei. *Semin. Cell Dev. Biol.* **78**, 107-115.

Ronneberger, O., Liu, K., Rath, M., Rueβ, D., Mueller, T., Skibbe, H., Drayer, B., Schmidt, T., Filippi, A., Nitschke, R. et al. (2012). ViBE-Z: a framework for 3D virtual colocalization analysis in zebrafish larval brains. *Nat. Methods* **9**, 735-742.

Roy, A., de Melo, J., Chaturvedi, D., Thein, T., Cabrera-Socorro, A., Houart, C., Meyer, G., Blackshaw, S. and Tole, S. (2013). LHX2 is necessary for the maintenance of optic identity and for the progression of optic morphogenesis. *J. Neurosci.* **33**, 6877-6884.

Ryu, S., Holzschuh, J., Erhardt, S., Ettl, A.-K. and Driever, W. (2005). Depletion of minichromosome maintenance protein 5 in the zebrafish retina causes cell-cycle defect and apoptosis. *Proc. Natl. Acad. Sci. USA* **102**, 18467-18472.

Sakkou, M., Wiedmer, P., Anlag, K., Hamm, A., Seuntjens, E., Ettwiller, L., Tschöp, M. H. and Treier, M. (2007). A role for brain-specific homeobox factor Bsx in the control of hyperphagia and locomotory behavior. *Cell Metab.* **5**, 450-463.

Sander, J. D., Cade, L., Khayter, C., Reyon, D., Peterson, R. T., Joung, J. K. and Yeh, J.-R. J. (2011). Targeted gene disruption in somatic zebrafish cells using engineered TALENs. *Nat. Biotechnol.* **29**, 697-698.

Sapède, D. and Cau, E. (2013). The pineal gland from development to function. *Curr. Top. Dev. Biol.* **106**, 171-215.

Schott, R. K., Müller, J., Yang, C. G. Y., Bhattacharyya, N., Chan, N., Xu, M., Morrow, J. M., Ghenu, A.-H., Loew, E. R., Tropepe, V. et al. (2016). Evolutionary transformation of rod photoreceptors in the all-cone retina of a diurnal garter snake. *Proc. Natl. Acad. Sci. USA* **113**, 356-361.

Shainer, I., Buchshtab, A., Hawkins, T. A., Wilson, S. W., Cone, R. D. and Gothilf, Y. (2017). Novel hypophysiotropic AgRP2 neurons and pineal cells revealed by BAC transgenesis in zebrafish. *Sci. Rep.* **7**, 44777.

Simões, B. F., Sampaio, F. L., Loew, E. R., Sanders, K. L., Fisher, R. N., Hart, N. S., Hunt, D. M., Partridge, J. C. and Gower, D. J. (2016). Multiple rod-cone and cone-rod photoreceptor transmutations in snakes: evidence from visual opsin gene expression. *Proc. Biol. Sci* **283**, 20152624.

Snelson, C. D., Burkart, J. T. and Gamse, J. T. (2008a). Formation of the asymmetric pineal complex in zebrafish requires two independently acting transcription factors. *Dev. Dyn.* **237**, 3538-3544.

Snelson, C. D., Santhakumar, K., Halpern, M. E. and Gamse, J. T. (2008b). Tbx2b is required for the development of the parapineal organ. *Development* **135**, 1693-1702.

Talbot, W. S., Trevarrow, B., Halpern, M. E., Melby, A. E., Farr, G., Postlethwait, J. H., Jowett, T., Kimmel, C. B. and Kimelman, D. (1995). A homeobox gene essential for zebrafish notochord development. *Nature* **378**, 150-157.

Thisse, C. and Thisse, B. (1999). Antivin, a novel and divergent member of the TGFbeta superfamily, negatively regulates mesoderm induction. *Development* **126**, 229-240.

Thisse, C., Thisse, B., Schilling, T. F. and Postlethwait, J. H. (1993). Structure of the zebrafish snail1 gene and its expression in wild-type, spadetail and no tail mutant embryos. *Development* **119**, 1203-1215.

Walls, G. L. (1934). The reptilian retina. *Am. J. Ophthalmol.* **17**, 892-915.

Weidinger, G., Thorpe, C. J., Wuennenberg-Stapleton, K., Ngai, J. and Moon, R. T. (2005). The Sp1-related transcription factors sp5 and sp5-like act downstream of Wnt/beta-catenin signaling in mesoderm and neuroectoderm patterning. *Curr. Biol.* **15**, 489-500.

Yáñez, J., Busch, J., Anadón, R. and Meissl, H. (2009). Pineal projections in the zebrafish (Danio rerio): overlap with retinal and cerebellar projections. *Neuroscience* **164**, 1712-1720.

Yarnold, J. K. (1970). The minimum expectation in X^2 goodness of fit tests and the accuracy of approximations for the null distribution. *J. Am. Stat. Assoc.* **65**, 864.

Zang, J., Keim, J., Kastenhuber, E., Gesemann, M. and Neuhauss, S. C. F. (2015). Recoverin depletion accelerates cone photoresponse recovery. *Open Biol.* **5**, 150086.